Random walk approximation of fractional-order multiscaling anomalous diffusion

Yong Zhang and David A. Benson
Department of Geology and Geological Engineering, Colorado School of Mines, Golden, Colorado 80401, USA

Mark M. Meerschaert
Department of Statistics and Probability, Michigan State University, East Lansing, Michigan 48824, USA

Eric M. LaBolle
Department of Land, Air, and Water Resources, University of California, Davis, California 95616, USA

Hans-Peter Scheffler
Department of Mathematics, University of Siegen, Germany

(Received 30 May 2006; published 22 August 2006; publisher error corrected 25 August 2006)

Random walks are developed to approximate the solutions of multiscaling, fractional-order, anomalous diffusion equations. The essential elements of the diffusion are described by the matrix-order scaling indexes and the mixing measure, which describes the diffusion coefficient in every direction. Two forms of the governing equation (also called the multiscaling fractional diffusion equation), based on fractional flux and fractional divergence, are considered, where the diffusion coefficient and the drift vary in space. The particle-tracking algorithm is also extended to approximate anomalous diffusion with a streamline-dependent mixing measure, using a streamline-projection technique. In this and other general cases, the random walk method is the only known way to solve the nonhomogeneous equations. Five numerical examples demonstrate the flexibility, simplicity, and efficiency of the random walk method.

DOI: 10.1103/PhysRevE.74.026706 PACS number(s): 02.60.Cb, 05.40.Fb, 02.60.−x, 05.10.Gg

I. INTRODUCTION

Various forms of Lévy motion and Lévy walks, and their fractional-order governing equations, have been used to describe superdiffusive spreading of passive scalars in turbulent and chaotic flow [1,2], plasma [3,4], surface and ground water flow [5–8], and financial returns [9–11]. Many of these studies have not differentiated the superdiffusive rates in different directions, although the evidence of multiple scaling rates is clear in contaminant transport in heterogeneous material [12], including fractured rock [13]. The multiscaling space-fractional diffusion equation (FDE, described in detail in the next section), describes anomalous superdiffusion with added realism by not only allowing direction-dependent spreading rates, but also specifying magnitudes of diffusion that are arbitrarily assigned on the entire unit sphere in d-dimensions [12]. The diffusion operator owes its existence to the coarse-graining, or upscaling, that eliminates some of the detail of the fine-grained velocity field. If the underlying velocity field is inherently anisotropic or has embedded preferential directions, then the multiscaling diffusion operator is an appealing tool for predicting anomalous superdiffusion at the coarser scale. For nonhomogeneous problems, however, analytic solutions are unavailable and numerical methods are needed.

Numerous numerical methods have been developed recently to simulate superdiffusion embodied in a one-dimensional (1D) fractional-order diffusion equation, including the finite element method (FEM) [14,15], the method of lines [16], the explicit and the related semi-implicit method [17], the three-point approximation method [5], the mass balance method [6], and the implicit Euler finite difference method (FDM) [18–20]. Only a few methods have been proposed to solve the multidimensional FDE, including the alternative direction implicit finite difference method (ADI FDM) [21], the fast Fourier transform method [22], and the FEM [14]. Although these methods have successfully solved the 1D and/or 2D FDEs, they cannot solve the multiscaling FDE with an arbitrary mixing measure and space-dependent coefficients. As discussed in the following section, a general mixing measure and the local variation of transport coefficients will significantly improve our ability to capture real-world superdiffusion.

A random walk method was developed recently to approximate the 1D FDE [23]. It is superior in many ways to traditional numerical methods in solving large flow systems, since it is grid-free, can be applied to any underlying form of flow (velocity) field, and does not cause numerical dispersion for advection-dominated transport problems. As a Lagrangian method, the random walk also illustrates the dynamics of the physical process. Most importantly, the embedded Lagrangian algorithm can easily add particle retention in immobile phases in a manner similar to classical continuous time random walks (CTRW) [24,25].

The computational efficiency and the potential flexibility of the random walk method motivates us to extend it to the multiscaling FDE. The rest of this paper is organized as follows: In Sec. II, we extend the multiscaling FDE to general forms where the strength of the nonlocal spreading is allowed to vary with the local-scale heterogeneity of the transport coefficients. In Sec. III, we describe the random walk particle-tracking schemes for solving the multiscaling FDEs. Numerical examples are presented as demonstrations. In Sec. IV, the extension of the random walk method to the case with a streamline-dependent mixing measure is discussed and illustrated.

II. MULTISCALING FDES WITH SPACE-DEPENDENT PARAMETERS

To illustrate the properties of a multiscaling FDE, we give examples of the dispersion of an inert tracer in water moving through porous media, although other applications are found in branches of finance and physics [26]. The multiscaling FDE proposed by Meerschaert *et al.* [12] is

$$\frac{\partial C}{\partial t} = -v \cdot \nabla C + D\nabla_M^{\boldsymbol{H}^{-1}} C, \tag{1}$$

where $C=C(\vec{x},t)$ is the scalar concentration, v is the drift vector, D is a scalar dispersion coefficient, $\boldsymbol{H}^{-1}$ is the inverse of the scaling matrix providing the order and direction of the fractional derivatives, and $M=M(d\theta)$ is the mixing measure. The eigenvalues of the scaling matrix $\boldsymbol{H}$ are the Hurst index scaling coefficients $1/\alpha$ of the growth process. For reference, a classical Brownian motion has all eigenvalues $H_i=1/2$ and the diffusion term is the Laplacian. The mixing measure, $M(d\theta)$, defines the shape and skewness of the plume in d-dimensions by assigning the strength of solute transport (or the probability of particle jumps) in each angular $d\theta$. The mixing measure may be either continuous or discrete, and $\int M(d\theta)=1$. The symbol $\nabla_M^{\boldsymbol{H}^{-1}}$ denotes the multiscaling fractional derivative, and this operator is understood by its Fourier transform [12]

$$F[\nabla_M^{\boldsymbol{H}^{-1}} C(\vec{x})] = \left[\int (e^{-i\vec{k}\cdot\vec{x}} - 1 + i\vec{k}\cdot\vec{x})\phi(d\vec{x})\right]\hat{C}(\vec{k}),$$

where $\phi(dy)$ is the intensity or Lévy measure [27], and $\phi(dy)=r^{-2}drM(d\theta)$ where $y=r^{\boldsymbol{H}^{-1}}\theta$ are the multiscaling polar coordinates. This is essentially a convolution of the function $C(\vec{x})$ with the Lévy measure, which satisfies the multiscaling relationship $c\phi(d\vec{x})=\phi(c^{-\boldsymbol{H}}d\vec{x})$ for any $c>0$ [12].

Some examples of this operator are well known. In 1D, and in the range of interest between ballistic and diffusive behavior $1<\alpha\leqslant 2$, the above Fourier transform reduces to $[p(ik)^\alpha+q(-ik)^\alpha]\hat{C}(k)$ with inverse transform $p\frac{d^\alpha C(x)}{dx^\alpha}+q\frac{d^\alpha C(x)}{d(-x)^\alpha}$, where $p+q=1$ are the mixing measure weights in the positive and negative directions. Also in 1D, the Riesz fractional derivative is recovered when $p=q=1/2$, giving the Fourier transform pair $\cos(\pi\alpha/2)|k|^\alpha\hat{C}(k) \Leftrightarrow \cos(\pi\alpha/2)\frac{d^\alpha C(x)}{d|x|^\alpha}$. The Riesz derivative is also symmetric in multiple dimensions in two ways. First, the order of the differentiation is equal in all directions, so that $\boldsymbol{H}^{-1}=\alpha\boldsymbol{I}$ (where $\boldsymbol{I}$ is the identity matrix), and $M(d\theta)$ is a uniform measure on the unit sphere. Then the multiscaling diffusion operator reduces to the Riesz fractional Laplacian defined by the Fourier transform pair (ignoring the leading constants) $\|\vec{k}\|^\alpha\hat{C}(\vec{k}) \Leftrightarrow \Delta^{\alpha/2}C(\vec{x})$ [12,28].

The FDE (1) allows a general mixing measure and scaling matrix, which is critical in applications such as the prediction of solute transport through heterogeneous porous media or fracture networks [12,13,22]. A realistic plume may grow at different rates along different, not necessarily orthogonal, directions, due to a possibly anisotropic depositional or structural geologic environment. Direction-dependent spreading rates are described by the scaling (Hurst) matrix [22]. In addition, a realistic plume may exhibit preferential flow and strength of dispersive flux in certain directions (corresponding to areas of higher permeability derived from paleochannels or fractures) which can be captured by the mixing measure. The FDE (1), however, only gives the governing equation for diffusion with constant characteristic coefficients [v, D, and $M(d\theta)$]. A FDE with space-dependent characteristic coefficients may significantly extend the ability of the constant-parameter FDE to capture the realistic plume evolution in regional-scale aquifers where the subsurface heterogeneity distribution tends to be nonstationary and the 3D geometry of local-scale heterogeneity is critical to solute transport. Here we extend the multiscaling FDE with constant characteristic coefficients [12] to one with space-dependent coefficients, and then develop the correspondent random walk approximations in the next section.

Using fractional flux in the first-order mass conservation law [29], we get the following multiscaling, FF-DE (where the "FF" denotes the fractional flux)

$$\frac{\partial C}{\partial t} = -\nabla\cdot[v(\vec{x},t)C] + \nabla\cdot[D(\vec{x},t)\nabla_M^{\boldsymbol{H}^{-1}-\boldsymbol{I}}C]. \tag{2}$$

In one dimension, Eq. (2) reduces to the 1D fractional advection-dispersion equation proposed by Zhang *et al.* [23], which corresponds to the fractional Fokker-Planck equation proposed by Tsallis and Lenzi [30]. A similar form has also been derived by other means [31]. When v and D are constant in space, Eq. (2) reduces directly to the multiscaling FDE (1).

Conversely, by taking the integer flux in the fractional-order mass conservation law [32], we get the following multiscaling, FD-DE (where the "FD" denotes the fractional divergence)

$$\frac{\partial C}{\partial t} = -\nabla\cdot[v(\vec{x},t)C] + \nabla_M^{\boldsymbol{H}^{-1}-\boldsymbol{I}}\cdot[D(\vec{x},t)\,\nabla\, C]. \tag{3}$$

If the solute concentrations at the domain boundaries are negligible and v and D is constant in space, Eq. (3) reduces to Eq. (1).

The dispersion term in the FD-DE (3) can also be derived by taking the adjoint of the dispersive flux in the FF-DE (2) [23]:

$$\{\nabla\cdot[D(\vec{x},t)\nabla_M^{\boldsymbol{H}^{-1}-\boldsymbol{I}}C]\}^* = -\nabla_{\bar{M}}^{\boldsymbol{H}^{-1}-\boldsymbol{I}}\cdot[D(\vec{x},t)\,\nabla\, C],$$

where $\bar{M}(d\theta)=M(d\theta+\pi)$, and the superscript asterisk denotes the adjoint operator (the classical integer-order adjoint method can be found in [33]).

Note the FF-DE (2) only considers the influence of local variation of dispersion coefficient D on the variation of solute flux, while the FD-DE (3) considers the influence of nonlocal variation of D. In the following section we develop random walk approximations for both FDEs, since currently there is no physical evidence to show that one is superior to the other.

III. RANDOM WALK ALGORITHMS AND NUMERICAL EXAMPLES

The following multiscaling compound Poisson process converges to operator Lévy motion [12,22]:

$$\vec{Z}(t) = \sum_{i=1}^{[t/dt]} \vec{X}_i = \sum_{i=1}^{[t/dt]} R_i^{\boldsymbol{H}} \cdot \vec{\theta}_i, \tag{4}$$

where $\vec{Z}(t)$ denotes the particle location at time t, $n=[t/dt]$ is the number of random jumps by time t using time step size dt, R_i is the random length of the ith jump and $P(R_i>r) \sim r^{-1}$, the jump direction $\vec{\theta}_i$ is a random unit vector drawn from the CDF of the mixing measure $M(d\theta)$ [see Eq. (5) below], and R_i and $\vec{\theta}_i$ are independent. The matrix $R^{\boldsymbol{H}}$ is anisotropic to allow different jump sizes in different directions.

In this section we will describe the distribution and generation of each $\vec{X}_i$ and will, for clarity, drop the subscript referring to individual jumps.

For a 2D case where the two eigenvectors of $\boldsymbol{H}$ are orthogonal (or in other words, the primary directions of growth are perpendicular), the operator stable exponent dictates independent jumps:

$$R^{\boldsymbol{H}} = \begin{bmatrix} R^{H_1} & 0 \\ 0 & R^{H_2} \end{bmatrix} = \begin{bmatrix} R^{1/\alpha_1} & 0 \\ 0 & R^{1/\alpha_2} \end{bmatrix}.$$

Since $P(R>r)=r^{-1}$ above some cutoff, the jump length probabilities on the kth eigenvector of $\boldsymbol{H}$ fall off as $P(R^{1/\alpha_k}>r)=r^{-\alpha_k}$. The jump length probabilities for trajectories off the eigenvectors decay like powers of a mixture of the scaling coefficients.

Assuming a discrete mixing measure M with n components (including the jump direction θ_j, with $j=1,2,\ldots,n$, and the correspondent intensity or probability M_j), the CDF of M_j, noted as p_m, can be calculated as

$$p_m = \sum_{j=1}^{m} M(d\theta_j), \quad \text{where } m = 1,2,\ldots,n. \tag{5}$$

A random number of $[0, 1]$ uniform distribution, U, is generated to help to determine the jump vector $\vec{X}$ of each particle at each time step:

$$\vec{X} = R^{\boldsymbol{H}} \cdot \vec{\theta}_m, \quad \text{if } p_{m-1} < U \leqslant p_m, \tag{6}$$

where the jump direction is preassigned as the direction of the mth angular θ_m in $M(d\theta)$, based on the range of U.

Next we calculate each component of the matrix $R^{\boldsymbol{H}}$ in Eq. (6). If D varies linearly in space and the governing equation is the FF-DE (2), the jump length of the particle along the eigenvector belonging to the kth eigenvalue $1/\alpha_k$ of $\boldsymbol{H}$ can be calculated by the formula [23]

$$R^{1/\alpha_k} = D(x_k)^{1/\alpha_k} dL_{\alpha_k}(t) + \Theta(\alpha_k - 1)^{1/(\alpha_k - 1)} \times \left| \frac{\partial D}{\partial x_k} \right|^{1/(\alpha_k - 1)} dL_{\alpha_k - 1}(t), \quad k = 1, \ldots L, \tag{7}$$

where k represents the direction of the kth eigenvector of $\boldsymbol{H}$, L is the dimension of $\boldsymbol{H}$, $\Theta=\mathrm{sgn}(\partial D/\partial x_k)=1$ if $\partial D/\partial x_k>0$ and -1 otherwise, and $dL_\alpha(t)$ and $dL_{\alpha-1}(t)$ denote the random noises underlying α-order and $(\alpha-1)$-order Lévy motions, respectively. Here $dL_{\alpha_1}, dL_{\alpha_2}, \ldots, dL_{\alpha_L}$ are maximally skewed, standard, α_k-stable random variables (see Appendix A) with distribution $S_{\alpha_k}(\sigma=1,\beta=+1,\mu=0)$ that can be generated directly using the modified Chambers-Mallows-Stuck (CMS) method (for details, see [23,34]). In 1D, Eq. (7) reduces to the Markov process that solves the 1D fractional diffusion equation with variable dispersion coefficient [see Eq. (14) in [23]].

Central limit theory [35] allows us to use a more efficient approximation of R^{1/α_k} in Eq. (7) using

$$R^{1/\alpha_k} = [D(x_k)dt]^{1/\alpha_k} \xi_{\alpha_k} + \Theta[(\alpha_k - 1)dt]^{1/(\alpha_k - 1)} \times \left| \frac{\partial D}{\partial x_k} \right|^{1/(\alpha_k - 1)} \xi_{\alpha_k - 1}, \tag{8}$$

where ξ_{α_k} (or ξ_{α_k-1}) denotes a centered (mean-zero for $\alpha>1$) and scale-one random jump length governed by a power law or Pareto probability density function proportional to $r^{-\alpha_k-1}$ (or $r^{-\alpha_k-2}$) for large jumps r. Provided that the ξ_{α_k} are properly scaled and shifted, the sum of these random jumps converges to the required α-stable $S_{\alpha_k}(\sigma=1,\beta=+1,\mu=0)$ based on the generalized central limit theorem [[35], Corollary 8.2.9]:

$$\frac{\xi_1 + \xi_2 + \cdots + \xi_n}{n^{1/\alpha_k}} \Rightarrow Y \sim S_{\alpha_k}(\sigma = 1, \beta = +1, \mu = 0), \tag{9}$$

where $n=t/dt$ is the number of time steps. The scale and shift constants needed in the calculation of ξ_{α_k} are shown in Appendix A. The accuracy improves for a larger number of time steps; in practice, more than ten time steps, or individual jumps, should be used for each particle (Appendix A).

Similarly, if $D(x)$ is first order differentiable (not limited to be linear) and the governing equation is the FD-DE (3), the random jump length is [23]

$$R^{1/\alpha_k} = D(x_k)^{1/\alpha_k} dL_{\alpha_k}(t) + \Theta \left| \frac{\partial D}{\partial x_k} \right|^{1/(\alpha_k - 1)} dL_{\alpha_k - 1}(t), \tag{10}$$

which is approximated by

$$R^{1/\alpha_k} = [D(x_k)dt]^{1/\alpha_k} \xi_{\alpha_k} + \Theta \left| \frac{\partial D}{\partial x_k} dt \right|^{1/(\alpha_k - 1)} \xi_{\alpha_k - 1}. \tag{11}$$

A different coefficient on the right-hand side (RHS) of Eq. (10) compared to Eq. (7) is needed to account for the difference between the two fractional diffusion equations (2) and (3). When D is a constant in space, the last term in both Eqs. (7) and (10) disappears and they reduce to the same random walk process for solving the homogeneous FDE (1). The random jumps shown here only represent the dispersive flux. The drift due to mean velocity (which may be along a different direction) can always be incorporated directly to the particle trajectory before the dispersion is calculated, as is done for the classical second-order diffusion process [36].

The decision to use either Eq. (7) or Eq. (8) to generate a single particle jump when solving the FF-DE (2) depends on

the potential dependence between each of the R^{1/α_k} corresponding to each eigenvector of $\boldsymbol{H}$. When the R^{1/α_k} are "correlated" to each other (which is not defined due to infinite variance) we select Eq. (8) where the random variables ξ_{α_k} can be generated by taking fractional powers of a single heavy-tailed variable that is generated by either the Pareto method or the fractional power method (Appendix A). The R^{1/α_k} are dependent when a particle is directed by the mixing measure to embark on a jump in between the eigenvectors. This method is required in Example 1 discussed in the next section. When the R^{1/α_k} are independent of each other (for instance, when the mixing measure is concentrated on eigenvectors of scaling matrix), we can use either Eq. (7) or Eq. (8). The same distinction between Eqs. (10) and (11) arises when solving the FD-DE (3).

Equation (6) is the generalized random walk formula for all scaling matrices and mixing measures. For cases where the scaling matrix and the mixing measure have special properties (such as orthogonal eigenvectors of $\boldsymbol{H}$ discussed in the next section), Eq. (6) can be simplified significantly, resulting in more efficient random walk algorithms.

The random walk algorithm is tested by four numerical examples described in the following sections. For the purpose of cross-verification, simple cases had to be selected so that other numerical or semianalytic methods can be applied or developed. However, the application of the random walk algorithm is not limited to the cases discussed below. Also note that in this section we restrict our attention to the constant-in-space mixing measure $M(d\theta)$ and scaling matrix $\boldsymbol{H}$. An extension to a spatially variable mixing measure is discussed later in this paper.

A. Example 1: Orthogonal eigenvectors in H and arbitrary mixing measure $M(d\theta)$

In typical heterogeneous porous media one can only estimate, predict, or measure the scale indexes along limited directions, such as the one parallel to the flow direction or perhaps the depositional stratigraphic directions. The contaminants, however, can always move along preferential pathways, which may depend on local connectivity of highly permeable materials and may be quite different from the primary stratigraphic directions.

For a 2D, diagonal $\boldsymbol{H}$, the scaling directions may be aligned with the Cartesian coordinates (where the growth rates are denoted α_x and α_y, with the subscripts x and y denoting the two Cartesian coordinate axis). If there are several arbitrary directions θ in the mixing measure (see, e.g., the operator stable parameters in Fig. 1), the jump vector $\vec{X}=[X,Y]$ (at each time step) defined by Eq. (6) has the following two components:

$$X = R^{1/\alpha_x} \cos\,\theta_m, \tag{12a}$$

$$Y = R^{1/\alpha_y} \sin\,\theta_m, \tag{12b}$$

if $p_{m-1} < U \leqslant p_m$. Here the jumps X and Y are along the directions of the eigenvectors belonging to the eigenvalues $1/\alpha_x$ and $1/\alpha_y$ of $\boldsymbol{H}$, respectively, and they are fractional powers of each other. So R^{1/α_x} depends on R^{1/α_y}, and we use

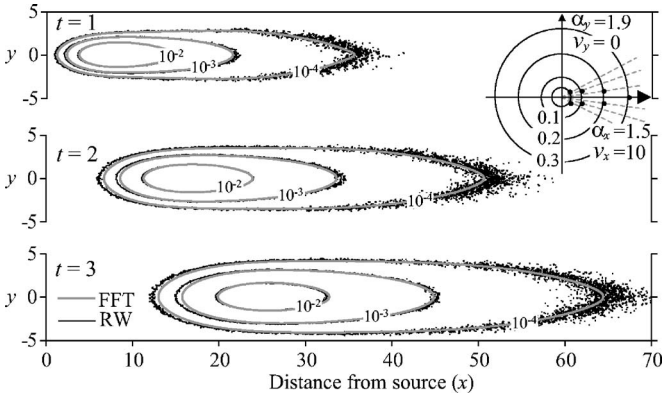

FIG. 1. Example 1: Simulated plumes at times $t=1$, 2, and 3 using the present random walks (dark lines) versus the semianalytical solutions using the FFT method (light lines). The Green function solutions of Eq. (1) are operator-stable density functions. The mixing measure has points at 0°, ±6°, ±12°, and ±18°, with increasing intensity in the direction of mean travel (polar plot). The initial condition is a Dirac delta function at $x=y=0$. The rough appearance of the random walk method is due to a fine ($\Delta x=0.1$) spatial discretization for particle number density counting.

Eq. (8) in the case of FF-DE [or Eq. (11) in the case of FD-DE] to calculate each $R^{1/\alpha}$. There are specific cases that the formula (12) can be simplified further. For instance, when the θ_m is aligned with the x axis, we have $X=\pm R^{1/\alpha_x}$ and $Y=0$, so the particle travels along the x axis only, with the jump pdf controlled by a α_x-order Lévy motion. Similarly, when θ_m is aligned with the y axis, we have $X=0$ and $Y=\pm R^{1/\alpha_y}$, so the particle travels along the y axis only, with the jump pdf controlled by a α_y-order Lévy motion. Examples of these two specific cases will be discussed in Sec. III C.

In this example, the velocity ($v_x=10$, $v_y=0$) and the dispersion coefficient ($D=1$, see Fig. 1) must be constant in order to compare with a known solution. To the best of our knowledge, the fast Fourier transform (FFT) method [22], which is limited to constant parameters, is the only other method available to solve this problem. Now the governing equation is simplified to the multiscaling FDE (1). The random walk solution (Fig. 1) is verified by the semianalytical FFT solution of the operator stable density Green functions of Eq. (1). This example has been suggested [12,22] as a means to explain different spreading rates and highly skewed spreading in heterogeneous aquifer material. The exchange rates of different currencies have also been shown to have operator stable growth characteristics [37].

B. Example 2: Nonorthogonal eigenvectors in H and $M(d\theta)$ concentrated on eigenvectors

In this example, the scaling matrix contains nonorthogonal eigenvectors, whose directions coincide with the only nonzero angular directions in the discrete mixing measure. It may represent the plume growth in a fractured aquifer where the fractures are limited to two dominant directions. The mixing measure and the scaling matrix in such a media would have the same directions, since (1) the migration of

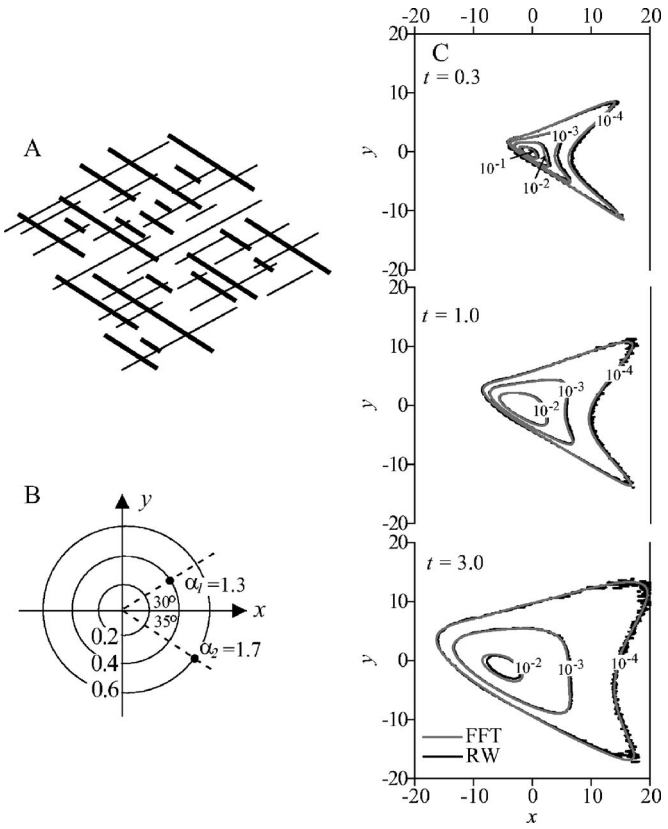

FIG. 2. Example 2: Random walk approximations of plume growth in a fractured aquifer. The velocity $v_x=v_y=0$, and the dispersion coefficient $D=1$. The governing equation is the multiscaling FDE (1). The initial condition is a Dirac delta function with the instantaneous point source located at the origin. (a) Noncontinuum conceptual model, (b) approximate operator stable parameters, and (c) the evolution of simulated particle plume concentrations, which also represent operator stable densities with time. The random walk (RW) solution is shown with dark lines, and the fast Fourier transform (FFT) method [22] is shown with light lines.

tracers (particle jumps) would be confined to the fracture networks, and (2) the fractures in each set may follow a fractal hyperbolic distribution, leading to dominant scaling directions that correspond to the fracture directions [13]. Now Eq. (6) can be simplified significantly:

$$\vec{X} = R^{1/\alpha_m}, \quad \text{if } p_{m-1} < U \leqslant p_m, \tag{13}$$

where $\vec{X}$ is along the direction of the eigenvector belonging to the eigenvalue $1/\alpha_m$ of $\boldsymbol{H}$. The jump vectors R^{1/α_m} along each eigenvector are independent. Here $m=1,\ldots,d$, where d is the dimension, which is also equivalent to the number of eigenvectors of the scaling matrix. So we can use either Eq. (7) or Eq. (8) to solve the FF-DE (2), or either Eq. (10) or Eq. (11) to solve the FD-DE (3). Method (7) was used in Fig. 2.

For lack of another solution method for the inhomogeneous problem, we consider space-constant velocity ($v_x=v_y=0$) and dispersion coefficient ($D=1$). Assuming that fractures occur at 30° and −35°, which are also the only nonzero parts defined in $M(d\theta)$, with eigenvalues $1/\alpha_1=1/1.3$ and $1/\alpha_2=1/1.7$, then the eigenvectors will be $\begin{bmatrix}\sqrt{3}/2\\ 1/2\end{bmatrix}$ and $\begin{bmatrix}0.819\\ -0.574\end{bmatrix}$, and the scaling matrix $\boldsymbol{H}$ will be $\begin{bmatrix}0.688 & 0.141\\ 0.0579 & 0.670\end{bmatrix}$. The numerical result is shown in Fig. 2. The random walk solutions of the multiscaling FDE (1) are verified by the numerical solutions using the FFT of the operator-stable density Green's functions of Eq. (1). Note again the random walk method will allow space-dependent v and D, while the FFT method will not.

C. Example 3: Orthogonal eigenvectors in $\boldsymbol{H}$, $M(d\theta)$ concentrated on the eigenvectors, and variable coefficients

This example is representative of solute transport through a structured aquifer with different spreading rates along the longitudinal, transverse, and/or vertical directions. The random walk algorithm is similar to that of Example 2. The subtle difference is that here the particle has the same probability of jumping along each Cartesian axis. In other words, $p_m=1/d$, for $m=1,\ldots,d$, where d is the dimension.

For comparison, we extend Meerschaert *et al.*'s ADI FDM [21] for space-variable parameters (see Appendix B), and solve the FF-DE (2) with both the extended ADI FDM method and the random walk method (Fig. 3). Two cases with different space-dependence of D are considered. Case 1 contains a constant-in-space D [Fig. 3(a)], while case 2 has a $D(x,y)$ increasing linearly with distance [Fig. 3(b)]. The ADI FDM cannot capture a nonorthogonally spreading plume, and thus it cannot be used for any other examples discussed in this study. It is also easy to simulate the results in Fig. 3(a) (with constant coefficients) using semianalytic methods that generate 1D α-stable densities. The solution is a bivariate stable with independent components. Therefore multiplying 1D stable densities laid out along the eigenvector directions will give the same result. However, this method cannot be used with space-variable transport coefficients, such as those shown in Fig. 3(b).

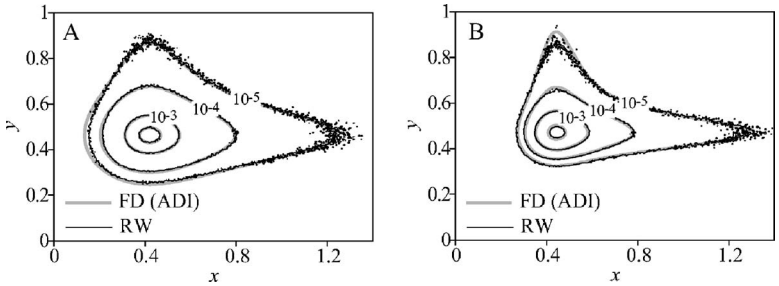

FIG. 3. Example 3: Numerical solutions for the 2D FF-DE (2), with the random walk (RW) method (dark lines) vs the implicit Euler finite difference method [FD (ADI), light lines]. The parameters are $\alpha_x=1.6$, $\alpha_y=1.8$, $t=1$, and the source is located at $x_0=y_0=0.48$. In (a), $D(x)=0.02$, $D(y)=0.005$; while in (b), $D(x)=0.02x$, $D(y)=0.005y$.

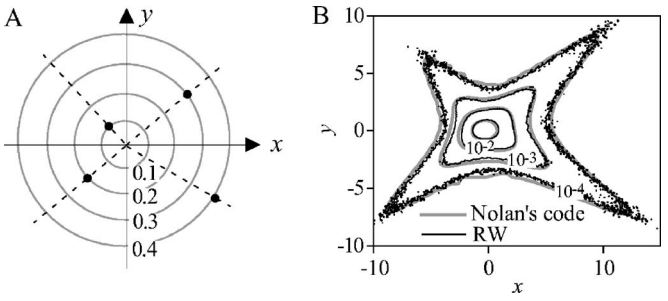

FIG. 4. Example 4: Solutions, at $t=1$, of the multidimensional FDE (14) (α is equal in all directions). (a) Polar plot of the discrete mixing measure showing four directions and weights. (b) Random walk solution (dark lines) vs Nolan's [38] multivariate stable distribution (light lines).

D. Example 4: Nolan's [38] two-dimensional, nonsymmetric stable density

Nolan's two-dimensional, nonsymmetric stable density surface [38] corresponds to a scalar H (i.e., H is constant in all directions) and a mixing measure with nonsymmetric weights and arbitrary angles. The governing equation is the following multidimensional FDE (where $H^{-1}=\alpha$ is used to correspond with previous notation):

$$\frac{\partial C}{\partial t} = D\nabla_M^{\alpha} C. \tag{14}$$

The multiscaling space-fractional diffusion equation (1) without the drift term reduces to Eq. (14) as a special case, when $\boldsymbol{H}^{-1}=\alpha \boldsymbol{I}$. This fractional derivative is similar to the Riesz derivative in that it has the same fractional order in all directions, but it is not symmetric: the prefactor in any direction is given by the mixing measure $M(d\theta)$.

Now Eq. (6) can be simplified further by using

$$\vec{X} = R^{1/\alpha}, \quad \text{where the jump direction is } \theta_m$$

$$\text{if } p_{m-1} < U \leqslant p_m. \tag{15}$$

The 2D anomalous diffusion with a discrete spectral measure is first approximated by random walks and then verified by the multivariate stable distribution (Fig. 4) generated by Nolan's code "mvstable" (see [38] for the method). The stability index α equals 1.6. The spectral measure contains 4 point masses along the directions 40°, 130°, 220°, and 330°, with weights 0.3, 0.1, 0.2, and 0.4, respectively.

In general, the random walk solutions in these examples compare well with the results using other numerical methods. The random walk algorithm is easy to implement and is robust, since it can simultaneously incorporate all of the generalities of the multiscaling dispersion operator and allow space-dependent transport coefficients. This robustness is beyond the capability of the other methods developed to solve the multiscaling FDE.

IV. STREAMLINE-DEPENDENT MIXING MEASURE

The random walk method can also be extended to allow a spatially variable mixing measure. The variability of the mixing measure is not uncommon in hydrology. For example, the orientation and density of fractures may change in space due to deformation. The scaling factor of diffusion, D, may also vary in space due to local (such as zonal) variation of fracture geometry and connectivity. Furthermore, in classical (Fickian) dispersion in porous media, the major axis of the dispersion tensor is aligned with, and proportional to the magnitude of, the velocity vector, which may take any orientation depending on boundary pressures or pumping stresses. In this case, the dispersion parameters are streamline dependent. Generalizing to the fractional-order case, the eigenvectors of the fractional derivative and the weights in the mixing measure will not be fixed in space, but may vary with streamlines or orientation of $v(x)$. Consequently, in random walks, particles will randomly disperse along certain directions moving with the streamlines while the mean flow is advected along streamlines.

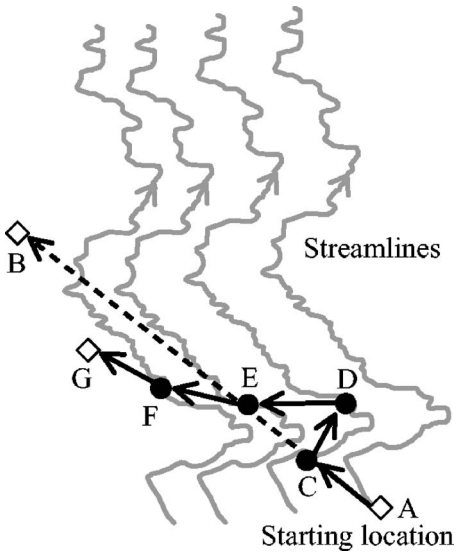

FIG. 5. Projection of one jump along adjacent streamlines. The meaning of points $A \sim G$ is explained in the text.

We propose a streamline-projection technique to account for the streamline-dependency of the mixing measure. As an illustration, 2D streamlines are shown in Fig. 5. At each time step, the particle (initially located at point A shown in Fig. 5) is assigned a random jump length L (with the ending point at B), and a random direction θ relative to the local velocity vector and the local mixing measure according to Eq. (6). However, along the trajectory, the particle's deviation from the streamline must be adjusted as it transfers to different streamlines. To simulate this, the length L is then cut into segments and projected into adjacent streamlines. The angle θ is adjusted according to the new direction of $v(x)$ and reprojected. The total length of the adjusted sum of segments is fixed at L.

The application of the projection method is demonstrated using one numerical example. A meandering 2D streamline (similar to a cycled sine function, representing the streamlines within a simplified meandering ancient river system) with free boundaries is shown in Fig. 6(a). To emphasize the effect of diffusion, here we turn off the mean advection. We consider the mixing measure with two directions moving

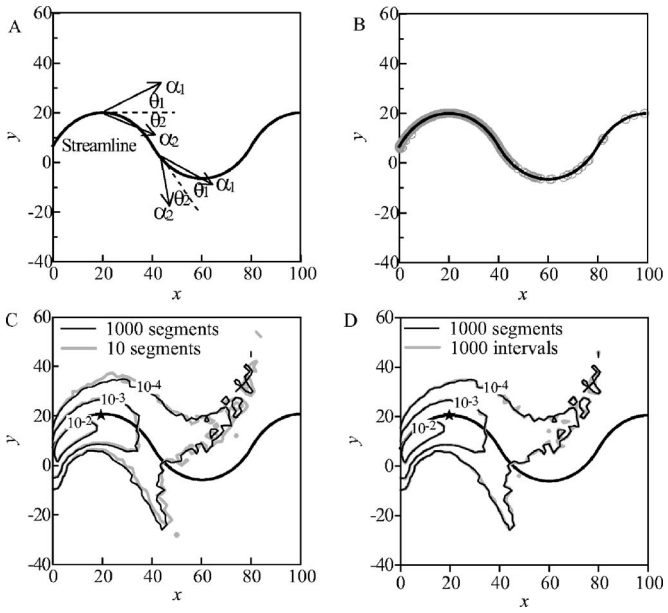

FIG. 6. (a) Streamline-dependent mixing measure. (b) Streamline (line) vs the particle plume (circles, representing 1000 particles), when the mixing measure has one point mass in the same direction as the streamline. (c) The simulated particle plume concentrations (normalized), with the number of equal-length segments equal to 10 (light lines) and 1000 (dark lines), respectively. (d) The simulated particle plume concentrations (normalized), with the number of equal-length segments equal to 1000 (dark lines) and the number of equal-time intervals equal to 1000 (light lines), respectively. The star in (c) and (d) represents the location of source, and the smooth curved lines are the streamline on which the source was placed.

with (relative to) the streamlines, as indicated by Fig. 6(a). Here one can divide each random particle jump (with the jump length L and the jump time dt) by cutting either the random jump length L or the jump time dt (note here dt is also the time step of the particle tracking algorithm). The first method is to cut L into equal-length segments, while the second method is to cut dt into equal-time intervals. Different numbers of cuttings may result in different final location of the particle, and thus the sensitivity of the particle location on the cutting number can be evaluated.

We first test the method with a specific case where the mixing measure has only one point mass parallel to the streamline. As expected, the projection method results in particle plumes with exactly the same shape as the streamline [Fig. 6(b)]. We next consider the mixing measure with two different directions, with $\theta_1=20°$ and $\theta_2=-15°$ [relative to $v(x)$], $M_1=0.3$ and $M_2=0.7$, $\alpha_1=1.2$ and $\alpha_2=1.7$, and $D=2$, respectively. The two directions (θ_1 and θ_2) move with the streamline, so the actual travel direction of the particle changes with space. We divide each jump into 10 and 1000 equal-length segments, respectively. Results show that the two simulated particle plumes (with the transport time $t=20$) are similar, with subtle differences at the leading edges [Fig. 6(c)]. The nuance at the leading edges is due to the higher sensitivity of larger jumps to the cutting number. In the second method, we cut each time step into 1000 equal-time intervals. Results show that the simulated particle plume is similar to that of the equal-length cutting method [Fig. 6(d)]. The similarity might be due to the large cutting numbers we used in both methods. When the cutting number is large, the equal-time cutting method is more computationally efficient since it takes fewer steps. Also note that in this example, the spreading rate α_1 (1.2) is much less than α_2 (1.7), resulting in a heavier leading edge along the θ_1 direction, even though the intensity M_1 is much less than M_2.

A direct verification of the projection method is impossible at present, due to the lack of analytical and other numerical solutions. However, this is also the motivation for developing this method. We anticipate that the method can be tested in a field setting, where both multiscaling dispersion [12] and space-variable parameters [39] have been suggested as important factors in the transport of tritium in an alluvial aquifer.

V. CONCLUSIONS

The multiscaling anomalous diffusion process governed by the multiscaling space-fractional diffusion equation can be approximated by simple random walks, with the particle-tracking algorithm depending on (1) the mixing measure, (2) the scaling matrix, and (3) spatial variability of the transport parameters. When the spreading rate along each angle of the mixing measure is defined explicitly, the multiscaling diffusion process can be approximated by independent random jumps along each angular direction of the mixing measure. When the angular directions of the mixing measure are no longer concentrated on the eigenvectors of the scaling matrix, the particle will jump under a mixture of spreading rates and the components of the jump along every eigenvector are powers of each other. In general, the particles move along each eigenvector of the scaling matrix with the PDF of displacement satisfying the density of a Lévy noise (whose scale index is defined by the eigenvalue of the scaling matrix), and the directional structure of particle plumes is captured by the mixture of motions in different directions described by the mixing measure.

Dependent random variables in the domains of attraction of α-stable random variables can be generated by taking fractional powers of either a stable or a modified Pareto random variable. The Pareto method converges faster and it is more computationally efficient than the traditional Chambers-Mallows-Stuck (stable) method since it needs only one random number. However, the stable method is more reliable than the Pareto method, since it does not hinge on the proper choice of density parameters.

The random walk method developed by this study is superior to other available numerical methods in characterizing real-world superdiffusion, since it allows not only a general mixing measure and scaling matrix, but also space-dependent characteristic coefficients.

The streamline projection method provides us the first approximation of the multiscaling anomalous diffusion with a streamline-dependent mixing measure. Numerical tests show that whether the jump is projected by cutting the jump length

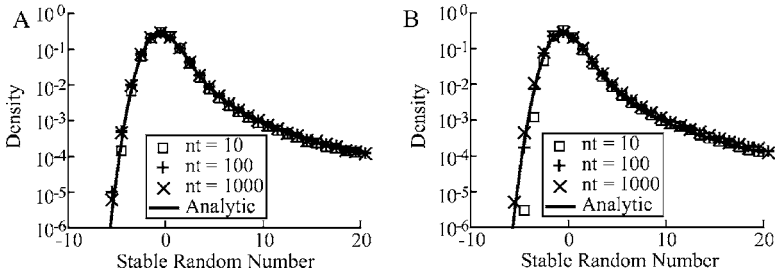

FIG. 7. The density of simulated $S_{1.7}(1,+1,0)$ random variables vs the analytical density using (a) the Pareto method and (b) the method of fractional power of the stable $S_{1.5}(1,+1,0)$. In the legends, "nt" denotes the number of sums, and "Ana" denotes the analytical solution.

or the jump time does not change the particle plume significantly, as long as the cutting number is sufficiently large.

ACKNOWLEDGMENTS

This material is based upon work supported by the National Science Foundation under Grant Nos. DMS-0417869, DMS-0539176, DMS-0139927, and DMS-0139943. Any opinions, findings, and conclusions or recommendations expressed in this material are those of the authors and do not necessarily reflect the views of the National Science Foundation. Z.Y. was also partially supported by Desert Research Institute.

APPENDIX A: NUMERICAL GENERATION OF DEPENDENT α-STABLE RANDOM VARIABLES

Both the original compound Poisson model (4) and the simplified jumps for a 2D orthogonal scaling matrix specified by Eq. (12) require us to generate dependent jump sizes along each eigenvector and then map that to the mixing measure. We develop and compare two different numerical methods to generate dependent α-stable random variables.

The first method is to take the fractional power of a known α_1-stable, and we denote it as the fractional power method. If R is a stable random variable with distribution $S_\alpha(\sigma=1,\beta=+1,\mu=0)$ (where σ denotes the scale parameter, β denotes the skewness, and μ denotes the shift; also see [40], p. 9, for the notation of distribution S), then sums of independent, identically distributed (iid) random variables distributed like $\mathrm{sgn}(R)|R|^{\alpha_2/\alpha_1}$ will converge to a stable with index α_2 and skewness +1, and the new variable $\mathrm{sgn}(R)|R|^{\alpha_2/\alpha_1}$ is (positively) correlated to R. Since we are unable to calculate the mean and scale parameter of $\mathrm{sgn}(R)|R|^{\alpha_2/\alpha_1}$ analytically, we estimate them numerically. We adopt the modified CMS method [34] to generate the α-stable $S_\alpha(1,+1,0)$ with the stability index $\alpha_1=1.5$, and then take their values to the α_2/α_1 power for all α_2 varying from 0.1 to 1.9. We then take the sums of *iid* random variables distributed like $[\mathrm{sgn}(R)|R|^{\alpha_2/\alpha_1}-\bar{\mu}]/\bar{\sigma}$ to approximate stables $S_{\alpha_2}(1,+1,0)$. Here the $\bar{\mu}$ is the estimated mean of $\mathrm{sgn}(R)|R|^{\alpha_2/\alpha_1}$. The $\bar{\sigma}$ is the estimated scale parameter of $\mathrm{sgn}(R)|R|^{\alpha_2/\alpha_1}$ adjusted based on Eq. (7.21) in [35] that is needed to approximate $\sigma=1$ stables with a fractional power. A histogram of sums of 1.7-stable variables generated by taking the fractional power of stable $S_{1.5}(1,+1,0)$ is shown in Fig. 7(b).

The second method is to take the sum of *iid* Pareto random variables, and we denote it as the Pareto method. Considering a Pareto distribution with the following density function

$$f(r)=\begin{cases} C\phi^{-1-\alpha}, & \text{if } q\leqslant r<\phi, \\ Cr^{-1-\alpha}, & \text{if } \phi\leqslant r<\infty, \end{cases}$$

where C is a (predefined) positive constant. The CDF is of the form

$$F(r)=\begin{cases} C\phi^{-1-\alpha}(r-q), & \text{if } q\leqslant r<\phi, \\ 1-(C/\alpha)r^{-\alpha}, & \text{if } \phi\leqslant r<\infty. \end{cases}$$

By assuming $F(r)=U$ where U is a uniform (0,1) random number, we can approximate r using

$$r=\begin{cases} \phi^{1+\alpha}U/C+q, & \text{if } U<C\phi^{-1-\alpha}(\phi-q), \\ [(1-U)\alpha/C]^{-1/\alpha}, & \text{if } U\geqslant 1-\phi^{-\alpha}C/\alpha. \end{cases}$$

The random variable distributed like $(r-\mu)/\sigma$ is in the domain of attraction of an α-stable random variable $S_\alpha(1,+1,0)$. Here $\mu=\frac{C}{2}\phi^{-1-\alpha}[\phi^2-q^2]+\frac{C}{\alpha-1}\phi^{-\alpha+1}$ is the mean of r, and $\sigma=\left[\frac{C\Gamma(2-\alpha)}{\alpha(1-\alpha)}\cos\frac{\pi\alpha}{2}\right]^{1/\alpha}$ is the scale parameter of r [according to Eq. (7.21) in [35]]. Note here that the value of ϕ, which is the cutoff of densities (from constant to the power-law form), significantly affects the rate of convergence. One example with $\alpha=1.7$ is shown in Fig. 7(a). An optimal $\phi=2.2$ is used. The efficiency of this method is obvious since the sums of only 10 Pareto random variables converge very closely to the true α-stable.

The simulated density of stable random variables using the Pareto method converges slightly faster to the analytical solution than that using the fractional power method. In addition, it takes four times less CPU time for the Pareto method than the fractional power method to finish one simulation. The relative computational inefficiency of the fractional power method is due to the tedious computational process of the original CSM method (see p. 50 in [34]). The fractional power method, however, is more reliable than the Pareto method, since it does not hinge on the proper choice of the cutoff of densities. Therefore we suggest using the fractional power method if the problem is relatively simple. Otherwise, the Pareto method is a better choice, if the cutoff is properly selected. Values near 2.0 are a good starting point for a wide range of α.

APPENDIX B: THE ADI FDM FOR SOLVING THE 2D ORTHOGONAL FF-DE (2)

The 2D, orthogonal FF-DE with the same jump intensity along the two axis is of the form

$$\frac{\partial C(x,y,t)}{\partial t} = \frac{\partial}{\partial x}\left[d(x,y)\frac{\partial^{\alpha-1}C(x,y,t)}{\partial x^{\alpha-1}} \right] + \frac{\partial}{\partial y}\left[e(x,y)\frac{\partial^{\beta-1}C(x,y,t)}{\partial y^{\beta-1}} \right] = d\frac{\partial^{\alpha}C}{\partial x^{\alpha}} + \frac{\partial d}{\partial x}\frac{\partial^{\alpha-1}C}{\partial x^{\alpha-1}} + e\frac{\partial^{\beta}C}{\partial y^{\beta}} + \frac{\partial e}{\partial y}\frac{\partial^{\beta-1}C}{\partial y^{\beta-1}}. \tag{B1}$$

It can be discretized as the implicit Euler approximation:

$$\frac{C_{i,j}^{n+1} - C_{i,j}^{n}}{\Delta t} = \frac{d_{i+1,j} - d_{i,j}}{\Delta x}\delta_{\alpha-1,x}C_{i,j}^{n+1} + d_{i,j}\delta_{\alpha,x}C_{i,j}^{n+1} + \frac{e_{i,j+1} - e_{i,j}}{\Delta y}\delta_{\beta-1,y}C_{i,j}^{n+1} + e_{i,j}\delta_{\beta,y}C_{i,j}^{n+1}, \tag{B2}$$

where the operators are

$$\delta_{\alpha-1,x}C_{i,j}^{n+1} = \frac{1}{(\Delta x)^{\alpha-1}}\sum_{k=0}^{i} g_k C_{i-k,j}^{n+1}, \tag{B3}$$

$$\delta_{\alpha,x}C_{i,j}^{n+1} = \frac{1}{(\Delta x)^{\alpha}}\sum_{k=0}^{i+1} f_k C_{i-k+1,j}^{n+1}, \tag{B4}$$

$$\delta_{\beta-1,y}C_{i,j}^{n+1} = \frac{1}{(\Delta y)^{\beta-1}}\sum_{k=0}^{j} K_k C_{i,j-k}^{n+1}, \tag{B5}$$

$$\delta_{\beta,y}C_{i,j}^{n+1} = \frac{1}{(\Delta y)^{\beta}}\sum_{k=0}^{j+1} L_k C_{i,j-k+1}^{n+1}, \tag{B6}$$

and the parameters g_k, f_k, K_k, and L_k are Grünwald weights.

According to the traditional ADI scheme, the equations are solved by two iterative steps [21]. At each new time step $n+1$, first we fix y and solve the problem in the x direction to obtain an intermediate solution $C_{i,j}^{*}$ from

$$\left[1 - \frac{\Delta t}{\Delta x}(d_{i+1,j} - d_{i,j})\delta_{\alpha-1,x} - \Delta t d_{i,j}\delta_{\alpha,x} \right] C_{i,j}^{\star} = C_{i,j}^{n}, \tag{B7}$$

and then we fix x and solve the problem in the y direction to obtain the solution $C_{i,j}^{n+1}$ from

$$\left[1 - \frac{\Delta t}{\Delta y}(e_{i,j+1} - e_{i,j})\delta_{\beta-1,y} - \Delta t e_{i,j}\delta_{\beta,y} \right] C_{i,j}^{n+1} = C_{i,j}^{\star}. \tag{B8}$$

The stability requirement is obtained based on the stability analysis for each 1D system. Here we use the matrix analysis method, which is similar to Appendix B in Zhang *et al.* [23], except that here we need not consider the advection. On the x-direction problem, Eq. (B7) can be written as

$$[F_y]C^{\star} = C^{n}. \tag{B9}$$

Similar to Eq. (36) in Zhang *et al.* [23], by choosing i so that $|x_i| = \max\{|x_l| : l = 0, 1, \ldots, N\}$, the eigenvalue of matrix $[F_y]$ is

$$\lambda = 1 - D_i\frac{\Delta t}{h^{\alpha}}\left[g_1 + \sum_{j=0, j\neq i}^{i+1} g_{i-j+1}\frac{x_j}{x_i} \right] - \frac{D_i - D_{i-1}}{\Delta x}\frac{\Delta t}{h^{\alpha-1}} \times \left[f_0 + \sum_{j=0, j\neq i}^{i-1} f_{i-j}\frac{x_j}{x_i} \right]. \tag{B10}$$

Note that $D_i = d_{ij}$ where j is fixed. Thus λ has real part exceeding 1 if

$$\mathrm{Re}\left\{ -D_i\frac{\Delta t}{h^{\alpha}}\left[g_1 + \sum_{j=0, j\neq i}^{i+1} g_{i-j+1}\frac{x_j}{x_i} \right] - (D_i - D_{i-1})\frac{\Delta t}{h^{\alpha}} \times \left[f_0 + \sum_{j=0, j\neq i}^{i-1} f_{i-j}\frac{x_j}{x_i} \right] \right\} \geqslant 0. \tag{B11}$$

By rearrangement, the above inequality is equivalent to

$$\mathrm{Re}\left\{ -D_i g_1 - (D_i - D_{i-1})f_0 + \sum_{j=0, j\neq i}^{i-1} [-D_i g_{i-j+1} - (D_i - D_{i-1})f_{i-j}]\frac{x_j}{x_i} - D_i g_0\frac{x_{i+1}}{x_i} \geqslant 0 \right\}. \tag{B12}$$

Therefore if $D_{i-1} < D_i$, an argument similar to Appendix A.2 in [23] shows that the finite difference equation will be stable. The same stability requirement can be found in the y-direction problem.

[1] M. F. Shlesinger, B. J. West, and J. Klafter, Phys. Rev. Lett. **58**, 1100 (1987).
[2] G. M. Zaslavsky, Physica D **76**, 110 (1994).
[3] D. del-Castillo-Negrete, B. A. Carreras, and V. E. Lynch, Phys. Rev. Lett. **91**, 018302 (2003).
[4] D. del Castillo-Negrete, B. A. Carreras, and V. E. Lynch, Phys. Plasmas **11**, 3854 (2004).
[5] Z. Deng, V. P. Singh, and L. Bengtsson, J. Hydraul. Eng. **130**, 422 (2004).
[6] X. X. Zhang, J. W. Crawford, L. K. Deeks, M. I. Stutter, A. G. Bengough, and I. M. Young, Water Resour. Res. **41**, W07029 (2005).
[7] B. Berkowitz and H. Scher, Phys. Rev. Lett. **79**, 4038 (1997).
[8] D. A. Benson, R. Schumer, M. M. Meerschaert, and S. W. Wheatcraft, Transp. Porous Media **42**, 211 (2001).
[9] E. Scalas, R. Gorenflo, and F. Mainardi, Physica A **284**,

376 (2000).
[10] F. Mainardi, M. Raberto, R. Gorenflo, and E. Scalas, Physica A **287**, 468 (2000).
[11] N. Laskin, Physica A **287**, 482 (2000).
[12] M. M. Meerschaert, D. A. Benson, and B. Baeumer, Phys. Rev. E **63**, 021112 (2001).
[13] D. M. Reeves, D. A. Benson, and M. M. Meerschaert, (unpublished).
[14] J. P. Roop, Ph. D. dissertation, Clemson University, 2004 (unpublished).
[15] V. J. Ervin and J. P. Roop, Numer. Methods Partial Differ. Equ. **22**, 558 (2006).
[16] F. Liu and I. Turner, J. Comput. Appl. Math. **166**, 209 (2004).
[17] V. E. Lynch, B. A. Carreras, D. del Castillo-Negrete, K. M. Ferreira-Mejias, and H. R. Hicks, J. Comput. Phys. **192**, 406 (2003).
[18] M. M. Meerschaert and C. Tadjeran, J. Comput. Appl. Math. **172**, 65 (2004).
[19] M. M. Meerschaert and C. Tadjeran, Appl. Numer. Math. **56**, 80 (2006).
[20] T. Tadjeran, H. P. Scheffler, and M. M. Meerschaert, J. Comput. Phys. **213**, 205 (2006).
[21] M. M. Meerschaert, H. P. Scheffler, and C. Tadjeran, J. Comput. Phys. **211**, 249 (2006).
[22] R. Schumer, D. A. Benson, M. M. Meerschaert, and B. Baeumer, Water Resour. Res. **39**, 1022 (2003)
[23] Y. Zhang, D. A. Benson, M. M. Meerschaert, and H. P. Scheffler, J. Stat. Phys. **123**, 89 (2006).
[24] E. W. Montroll and G. H. Weiss, J. Math. Phys. **6**, 167 (1965).
[25] H. Scher and M. Lax, Phys. Rev. B **7**, 4491 (1973).
[26] R. Metzler and J. Klafter, J. Phys. A **161**, 16 (2004).
[27] J. Bertoin, *Lévy Processes* (Cambridge Univ. Press, New York, 1996).
[28] M. M. Meerschaert, D. A. Benson, and B. Baumer, Phys. Rev. E **59**, 5026 (1999).
[29] R. Schumer, D. A. Benson, M. M. Meerschaert, and S. W. Wheatcraft, J. Contam. Hydrol. **48**, 69 (2001).
[30] C. Tsallis and E. K. Lenzi, Chem. Phys. **284**, 341 (2002).
[31] J. H. Cushman and T. R. Ginn, Water Resour. Res. **36**, 3763 (2000).
[32] M. M. Meerschaert, J. Mortensen, and S. W. Wheatcraft, Physica A **367**, 181 (2006).
[33] W. Feller, *An Introduction to Probability Theory and Its Applications*, 2nd ed. (Wiley, New York, 1971).
[34] A. Janicki and A. Weron, *Simuation and Chaotic Behavior of α-stable Stochastic Processes* (Marcel Dekker, New York, 1994), p. 355.
[35] M. M. Meerschaert and H. P. Scheffler, *Limit Distributions for Sums of Independent Random Vectors: Heavy Tails in Theory and Pratices* (Wiley, New York, 2001), p. 484.
[36] E. M. LaBolle, J. Quastel, G. E. Fogg, and J. Gravner, Water Resour. Res. **36**, 651 (2000).
[37] M. M. Meerschaert and H. P. Scheffler, in *Recent Advances and Trends in Nonparametric Statistics*, edited by M. G. Akritas and D. N. Politis (Elsevier Science, New York, 2003).
[38] J. P. Nolan, in *A Practical Guide to Heavy Tails: Statistical Techniques and Applications*, edited by R. J. Adler, R. Feldman, and M. Taqqu (Birkhauser Boston, Cambridge, MA, 1998).
[39] S. Lu, F. J. Molz, and G. J. Fix, Water Resour. Res. **38**, 1165 (2002).
[40] G. Samorodnitsky and M. Taqqu, *Stable Non-Gaussian Random Processes* (Chapman & Hall, New York, 1994), p. 632.